

Electrochemical Corrosion and Mathematical Model of Cold Spray Copper Composite Coating - Part II: Limiting Current Region

Ding Rui¹, Yu Haibin^{1*}, Li Xiangbo²

¹ Ningbo Institute of Industrial Technology, Chinese Academy of Science, Ningbo 315201, China

² Science and Technology on Marine Corrosion and Protection Laboratory, Luoyang Ship Material Research Institute(LSRMI), Qingdao 266101, China;

*E-mail: d moyuyang@foxmail.com

Received: 18 October 2016 / Accepted: 2 December 2016 / Published: 30 December 2016

In this paper, Cu – Cu₂O composite coating was prepared by cold spray technique and the corrosion behavior of the coating in 3.5% NaCl solution was studied using rotating ring-disk electrode. Experiments were designed to investigate the influences of rotation rate, chloride ion concentration, solution temperature and Cu₂O content on the polarization behavior of the coating. The results shown that under strong convection and high temperature conditions, the cumulative effect of insoluble corrosion product CuCl weakened, corrosion current increased, and current peak disappeared gradually due to enhanced diffusion. Limiting current i_L and rotation rate ω were in a log-linear relationship. When the chloride ion concentration in the solution increased, large amounts of chlorine ions were complexed with insoluble CuCl to generate soluble $CuCl_2^-$. So limiting current increased, potential range of limiting current narrowed, and current peak disappeared gradually. Limiting current was also in a log-linear relationship with the Cl^- concentration. As cathode, Cu₂O particles in the coating promoted the corrosion of copper and the release of dissolved copper, which improved the antifouling efficacy of the coating. Limiting current was controlled by diffusion of $CuCl_2^-$, and limiting current generating mechanism was essentially the diffusion-controlled film dissolution mechanism. The mathematical model for limiting current region was built based on the reaction course proposed herein and agreed well with the experimental results, which proved the correctness of the reaction course hypothesis and the mathematical model.

Keywords: Cold spray, Electrochemical polarization, Antifouling, Corrosion, Mathematical model

1. INTRODUCTION

With the exploitation of marine resources and the development of aquaculture, coastal defense, waterway transport and coastal power plants, harms caused by marine biofouling have become

increasingly prominent. To date, the common method for preventing marine biofouling is application of antifouling paints. However, antifouling paints are faced with defects such as undesirable antifouling duration and film strength, while peeling of coating seriously affects the antifouling effect of paints [1-4].

Cold spray is a spraying technique based on the principles of aerodynamics. At lower temperature relative to thermal spraying, powder particles are carried into the convergent-divergent nozzle by high-pressure gas. Particles are accelerated to supersonic state of 300~1200 m/s after passing through the entire nozzle to form gas-solid dual-phase high-velocity particle flow. Particles impact the substrate in solid state, which are deposited on the substrate surface by producing large plastic deformation to form a coating [5-8]. With advantages like high density, high hardness and strong adhesion, application of cold spray coating in the antifouling field can eliminate the easily peeling defect of antifouling paints.

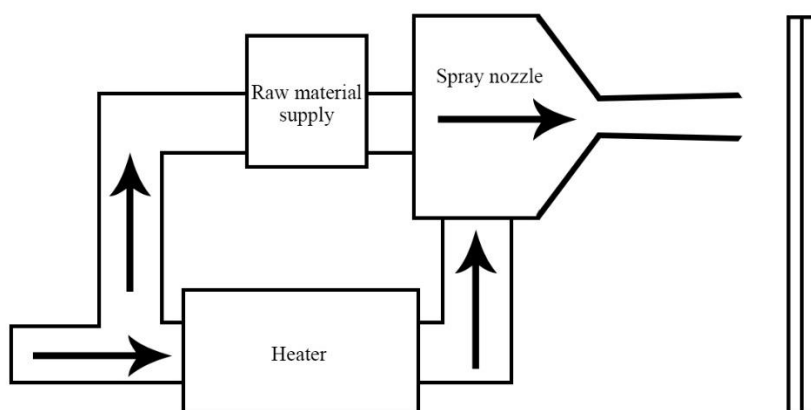


Figure 1. Schematic diagram of Cold Spray

In this paper, Cu – Cu₂O coating is prepared employing cold spray technique, and its antifouling performance is achieved by releasing Cu(I) and Cu(II) to surrounding water bodies. If the coating corrodes excessively fast to expose the steel substrate under it, its service life will be reduced. If the coating corrodes excessively slow, release rate of Cu (I) and Cu (II) will be less than the critical rate $10 \mu\text{g} \cdot \text{cm}^{-2} \cdot \text{d}^{-1}$, which will be unable to inhibit the adhesion of marine creatures. Therefore, research of its electrochemical behavior is very necessary [9-10]. Corrosion of copper and copper alloy in chloride-containing solution have been extensively studied [11-14], with three reaction mechanisms being developed and corresponding mathematical models for Tafel linear polarization region being established [15-31]. However, these mathematical models only contained the Tafel region, which did not involve the limiting current and high potential regions. In the previous studies, the authors investigated the features of Tafel region concerning the electrochemical polarization behavior of cold spray Cu – Cu₂O in 3.5% NaCl solution and established the mechanism for electrochemical reaction, as well as a polarization mathematical model of Tafel region based on this mechanism [9,10]. In this study, we continue to investigate the features of limiting current region with respect to the

electrochemical polarization behavior of the coating in 3.5% NaCl solution and build a polarization mathematical model of limiting current region based on the already-proposed mechanism.

2. EXPERIMENTAL METHODS

2.1 Preparation of cold spray coating

Coating used in the experiment was prepared by cold spray technique. The process parameters were as follows: spraying temperature of 300 °C; pressure of 2.8 MPa; and spraying distance of 20 mm. Coating materials were copper and Cu₂O powders, while substrate material was Q235 steel.

Cu particles used in this experiment were metallic yellow quasi-spherical particles. As can be seen from Figure 2, diameter of Cu powders was generally around 50 μm, with uniform distribution of particle size, smooth surface and good sphericity, which facilitated production of good quality coating as reported in reference 32.

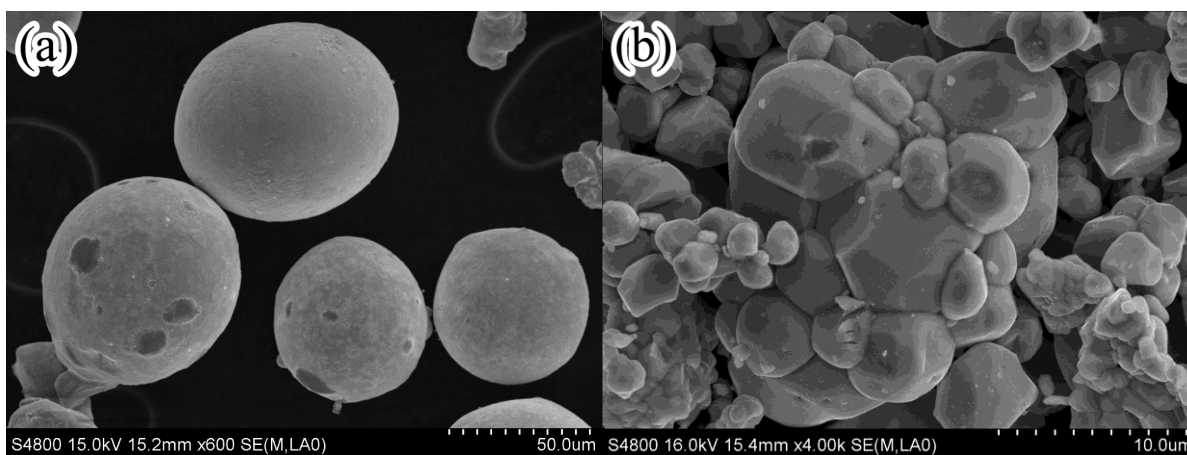


Figure 2. SEM image of (a) Cu powder and (b) Cu₂O powder

Cu₂O was dark red powders, which were mostly spherical, with dispersed distribution of particle size ranging from 1 μm to 10 μm, as shown in Figure 2. However, most of these particles aggregated to form 10 μm to 20 μm large particles. Reference 32 reported the influence of particle size on the deposition effect. Aggregation of Cu₂O powder particles increased their size above 10 μm, which was more conducive to the deposition of Cu₂O particles [2,32].

Coating composed of 10% Cu₂O + 90% Cu (mass ratio) was used as the experimental object in all experiments except for the experiment investigating the influence of Cu₂O content in the coating.

2.2 Sample processing

Sample prepared by cold spray was cut into disks with diameter of 5 mm. Then coating surface was polished slightly with 2000# sandpaper while avoiding wear through of the coating. Then, coating

surface was polished on the metallographic polisher sequentially with W5.0 and W2.5 diamond pastes, cleaned with alcohol moistened cotton ball, then dried and sealed for subsequent use.

2.3 Electrochemical testing system

Structure of the rotating ring-disk electrode used in the experiment has shown in reference 9. Experimental material, i.e. cold spray Cu – Cu₂O coating, was removable. Rotating ring-disk electrode parameters: disk diameter of 5 mm; ring-disk spacing of 1 mm; ring width of 1 mm; and collection efficiency of 31%.

The schematic diagram of the electrochemical testing system has shown in in reference 9. Rotation rate was controlled with Model 636 electrode rotator (Princeton, USA). Model PAR 2273 electrochemical workstation (Princeton, USA) was used for polarizing disk electrode, as well as recoding of disk electrode potential and current data. Ring electrode potential was set (at 600 mV for detection of cuprous ions, whereas at –100mV for detection of copper ions) with model DJS – 292B potentiostat (Xinrui Instruments Co., Ltd., Shanghai). Model PAR 273 electrochemical workstation (Princeton, USA) was used as the data recording system to record the ring electrode current data. Polarization process was scanned by potentiodynamic method at a rate of 0.333 mV/s.

2.4 Experiment influencing factors

In all the experiments concerning the influences of rotation rate ω and solution temperature T on the coating polarization, 3.5% NaCl solution was used. Temperature was controlled with constant temperature water bath.

In the experiment investigating the influence of rotation rate, ω was set at 200, 300, 650, 1300, 1900, 2500 and 3200 revolutions \cdot min⁻¹ (rpm), respectively.

In the experiment investigating the influence of Cl⁻, NaCl solutions with concentrations of 0.1, 0.2, 0.5, 1.0, 2.0, 3.0 and 4.0 mol \cdot L⁻¹ were used, at controlling temperature of 25 °C, pH of 8.0, and rotation rate of 1300 rpm.

2.5 Metallographic experiment and micro-area potential detection

Metallographs of Cu₂O particles and surrounding area in the coating immersed in 3.5% NaCl solution for different times were recorded during experiment, and corresponding micro-area potential distributions were detected. Experimental time was selected as 1st, 5th, 15th, 20th and 30th days after immersion. Model of metalloscope used was DMI 5000M (LEICA, Germany). Schematic diagram of the micro-area potential scanning system is shown in reference 1, which consisted of ACM electrochemical workstation (GillAC Co., UK), OPENSYS microscopic test platform and XMU-BY-1 automatic step controller (CBeing Nano-Instruments Co., China). Distance between probe and sample surface was 10 μ m, while scan rate was 2.5 s/line.

2.6 X-ray diffraction patterns

Phase analysis was performed on the coating before and after polarization using model D8 ADVNCE X-ray diffractometer (Bruker-AXS, Germany). Experimental parameters: diffraction source of Cu target; scanning range of 5-90°; scanning speed of 0.3 s/step; step size of 0.02°; working current of 40 mA; and working voltage of 40 mV.

3. EXPERIMENTAL RESULTS

In our previous study, the typical anodic polarization curve of cold spray copper composite coating was divided into three parts [9]:

- (1) Tafel active dissolution region ($\text{Cu} \rightarrow \text{Cu(I)}$);
- (2) Peak current and limiting current region 1 ($\text{Cu} \rightarrow \text{Cu(I)}$);
- (3) High potential region ($\text{Cu(I)}, \text{Cu}_2\text{O} \rightarrow \text{Cu(II)}$). High potential region further comprised two parts: (3-1) Current growth region and (3-2) limiting current region 2.

Among them, Tafel active dissolution region has previously been discussed [9]. This paper focuses on the peak current and limiting current region 1, while the high potential region will be discussed in the future work.

3.1 Influence of rotation rate

Figure 3 presents the anodic polarization curves of limiting current region 1 at different rotation rate. Current increased with increasing rotation rate. Meanwhile, current peak exhibited a narrowing trend with increasing rotation rate, indicating that at high rotational speeds, diffusion enhanced, and accumulation effect of CuCl weakened. As shown in Figure 4, log-slope between limiting current density i_L and rotation speed ω was 0.47.

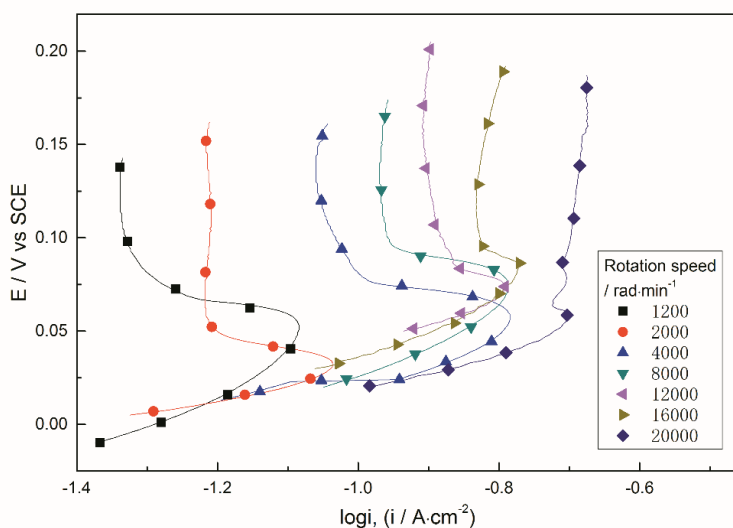


Figure 3. Anodic polarization curves in limiting current region 1 at different rotation rate (10% Cu_2O , 3.5% NaCl, 25°C)

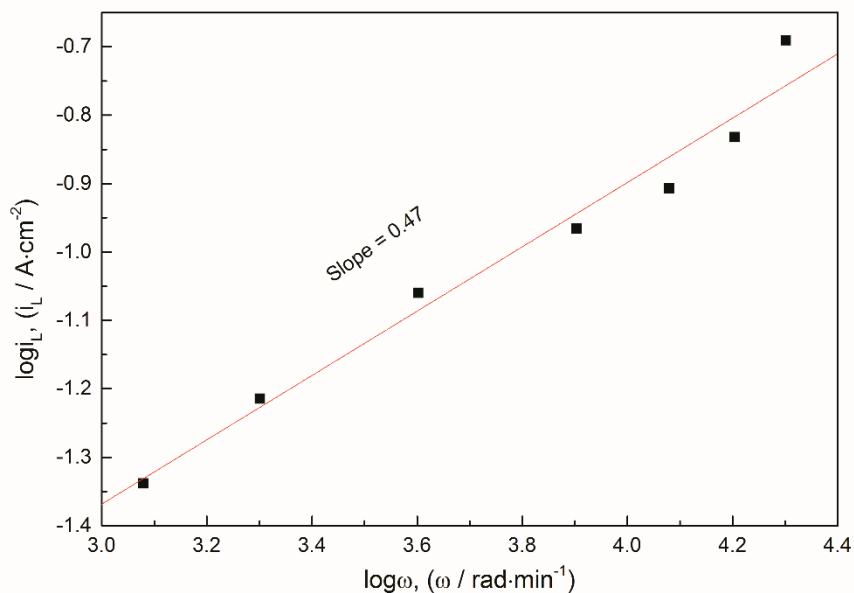


Figure 4. Log-linear relationship between i_L and ω (10% Cu_2O , 3.5% NaCl , 25°C)

3.2 Influence of Cl^- concentration

Figure 5 shows the polarization curve for limiting current region 1 at different Cl^- concentration. Limiting current i_L increased with increasing Cl^- concentration. In addition, at high chloride ion concentration, potential range of limiting current narrowed, and current peak disappeared gradually. This was because large amounts of Cl^- were complexed with insoluble CuCl to generate soluble CuCl_2^- , which led to weakened accumulation of CuCl . Limiting current i_L and Cl^- concentration were in a log-linear relation as shown in figure 6, with a slope of 0.886.

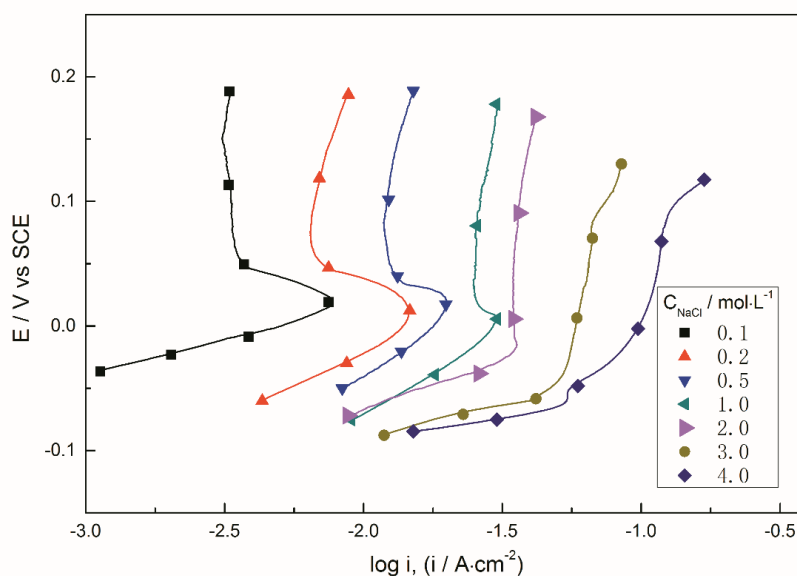


Figure 5. Anodic polarization curves in limiting current region 1 at different Cl^- concentration (10% Cu_2O , 8000 $\text{rad}\cdot\text{min}^{-1}$, 25°C)

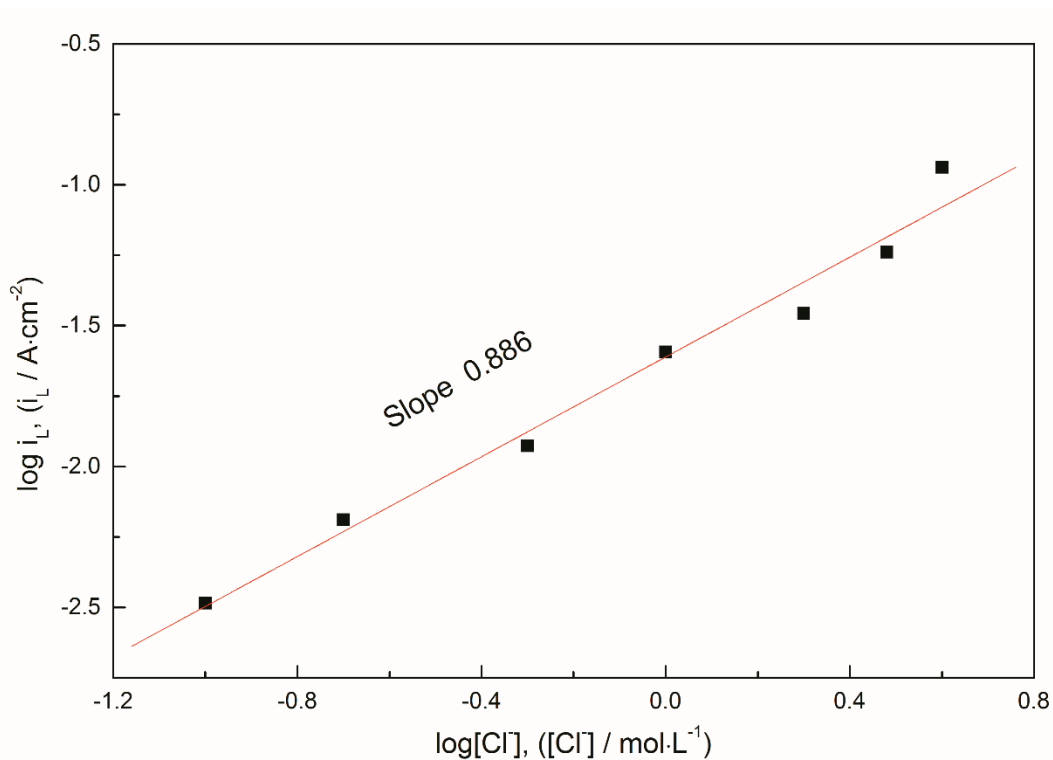


Figure 6. Log-linear relationship between i_L and Cl^- concentration (10% Cu_2O , $8000 \text{ rad}\cdot\text{min}^{-1}$, 25°C)

3.3 Influence of temperature

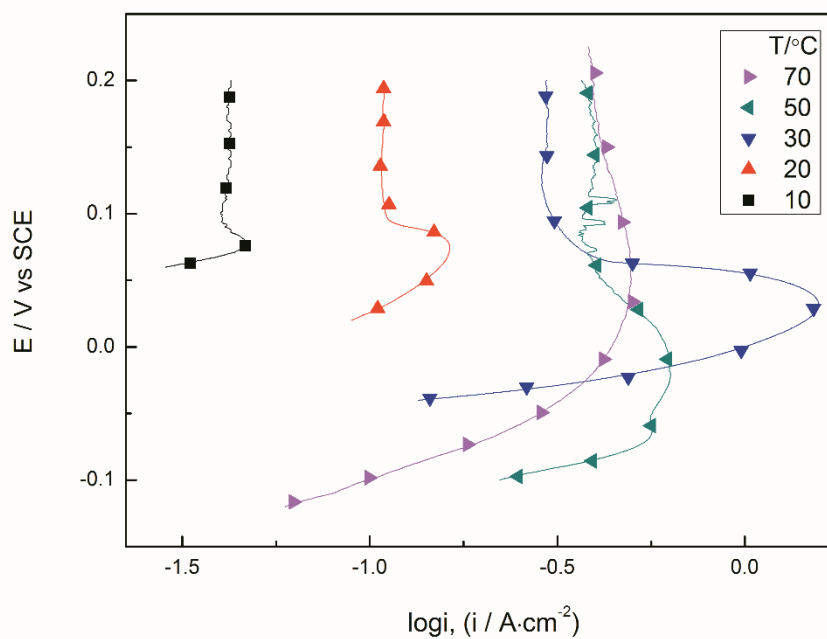


Figure 7. Anodic polarization curves of limiting current region 1 at different temperature (10% Cu_2O , 3.5% NaCl , $8000 \text{ rad}\cdot\text{min}^{-1}$)

Figure 7 shows the polarization curves for limiting current region 1 at different temperatures, where the limiting current increased with rising temperature. This may be because the rise of temperature accelerated the oxidation reaction of copper, which also increased the CuCl_2^- diffusion coefficient D and reduced the dynamic viscosity γ of the solution[33]. According to the convection-diffusion transfer flux formula $J = 0.62D^{2/3}\gamma^{-1/6}\omega^{1/2}c$ for rotating disk electrode derived by Levich [33], with increasing diffusion coefficient D , CuCl_2^- transfer flux J increased, and limiting diffusion current increased.

In addition, as the temperature rose, current peak first became apparent, and then disappeared gradually. This may be because the adsorption of corrosion product CuCl on the electrode surface was an endothermic process. Rise of temperature facilitated the adsorption, and the peak current region which reflected the adsorption process of CuCl was distinct. However, continuous rise of temperature would aggravate the thermal motion and complexation reaction of CuCl and Cl^- to inhibit the adsorption process, so the peak current disappeared gradually.

3.4 Role of Cu_2O

To study the role of Cu_2O in the electrochemical corrosion process of the coating, metallographic picture of Cu_2O particles and surrounding area in the coating immersed in 3.5% NaCl solution for different times were recorded and corresponding potential distributions were detected as shown in figure 8.

In the early stage of immersion, potential Cu_2O particles was high, which acted as cathode. Copper around the Cu_2O particles exhibited an annular low potential region, which existed as anode (Figure 8a). Cu_2O particles formed micro-battery with the surrounding copper to promote the corrosion of the later. With the prolongation of immersion time, peripheral region of Cu_2O particles formed an annular groove due to corrosion of copper and dissolution of cuprous oxide (Figure 8b). Since the copper ions hydrolyzed to form H^+ , and the anions in the solution migrated into the groove under the action of electric field, the solution within the groove became more corrosive. Hence, grooving corrosion expanded, anode region presented an expanding trend, and potential shifted towards more negative direction (Figure 8c). When immersed for 20 days, pitting corrosion was formed at the original location of Cu_2O particles (Figure 8d) as its exfoliation due to the corrosion of surrounding copper and its dissolution under the action of Cl^- . There was no longer the presence of Cu_2O cathode region in the potential distribution diagram (Figure 8d). Pits grew with the prolongation of immersion time (Figure 8e). As can be seen from Figure 8e, anode region expanded, and potential shifted to the negative direction.

Cu_2O is a main antifouling ingredient of traditional antifouling paints, which dissolves under the action of Cl^- to release Cu(I) and Cu(II) and suppress the adhesion of marine creatures [9,10]. Experimental results suggested that Cu_2O particles might also act as cathode to promote the corrosion of copper, release of dissolved copper ions, and improve the antifouling efficacy of the coating.

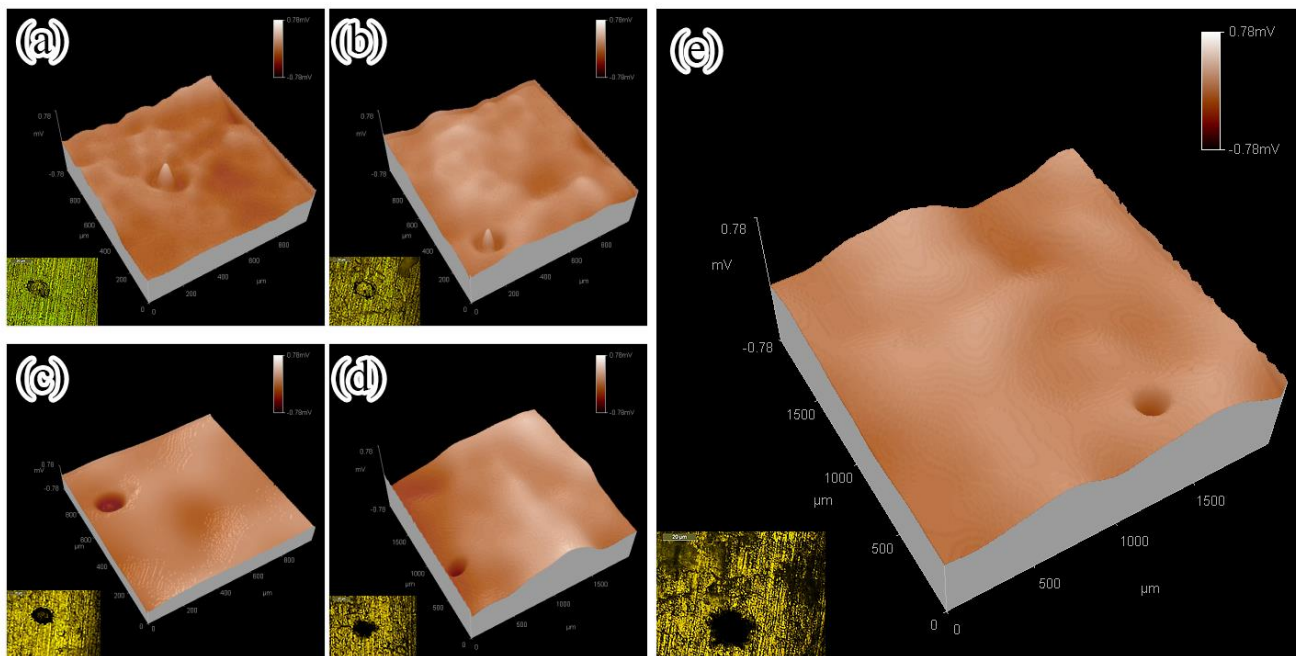


Figure 8. Metallographic picture and potential distribution of Cu_2O particles in the coating immersed for (a) 1 day, (b) 5 days, (c) 15 days, (d) 20 days, (e) 30 days in 3.5% NaCl solution (25°C)

3.5 Reaction mechanism

Electrochemical dissolution of copper and copper alloys in chlorinated solution has been extensively studied [15-31], with development of three different reaction mechanisms and the establishment of corresponding mathematical models for Tafel active dissolution region [19-31]. However, these reaction mechanisms and mathematical models all assumed the charge transfer process to be a quasi-reversible process, which tacitly approved the control step as a diffusion process and thus could not effectively reflect the real situation.

Figure 9 presents the XRD patterns of coating before and after polarization. Corrosion products were mainly CuCl and $\text{CuCl}_2 \cdot 2\text{H}_2\text{O}$, of which $\text{CuCl}_2 \cdot 2\text{H}_2\text{O}$ might be generated by oxidation and hydration of CuCl_2^- . Hence, we propose the following reaction mechanism.

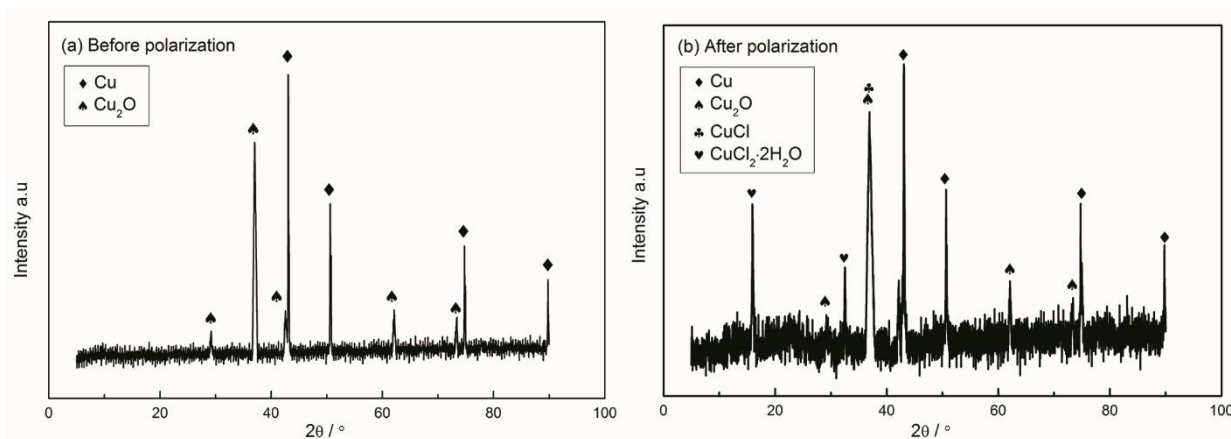


Figure 9. XRD patterns of the coating (a) before and (b) after polarization

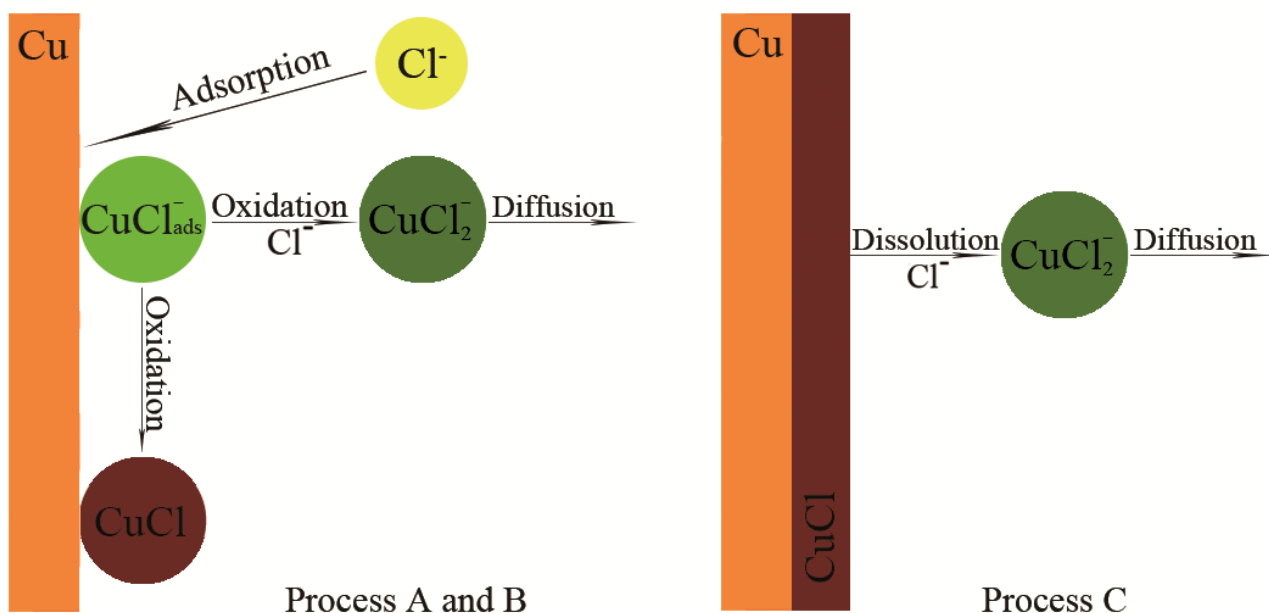


Figure 10. Schematic of the electrochemical reaction mechanism

When the coating was immersed in seawater, three processes proceeded sequentially on its surface: (A) chloride ion adsorption; (B) parallel competition between anodic dissolution and oxide film formation; and (C) dissolution of oxide film. These three processes are elaborated in detail below.

Process (A):

Cl⁻ adsorbed on the coating surface to form the transitional product CuCl_{ads}⁻:

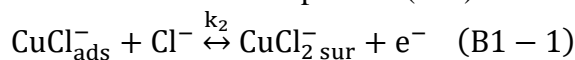


This reaction was a common initial step for the anodic dissolution and oxide film formation in process (B).

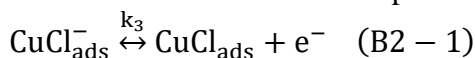
Process (B):

Transitional product CuCl_{ads}⁻ could proceed different reactions, i.e. different sub-processes: anodic dissolution process (B1) and oxide film formation (B2).

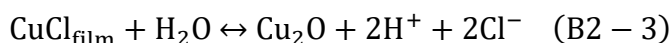
Firstly, CuCl_{ads}⁻ could further adsorb Cl⁻ and oxidize to convert to a soluble anodic oxidation product, which was precisely the anodic dissolution process (B-1).



Next, transitional product CuCl_{ads}⁻ no longer continued to adsorb Cl⁻ and could be directly oxidized to insoluble film, which was the oxide film formation process (B-2).



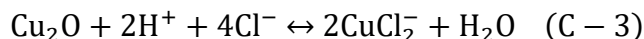
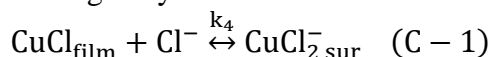
CuCl film further reacted to form Cu₂O film.



Anodic dissolution and oxide film formation processes were in a mutually competing, parallel reacting relationship.

Process (C):

Oxide film would also be damaged by H^+ and Cl^- in the solution to produce dissolution:



Which was precisely the dissolution process of oxide film.

3.6 Mathematical model for anodic limiting current region

Table 1. Symbol Description

k_4, k_{-4}	Chemical reaction equilibrium constant
r	Formation rate or Consumption rate
α	Transfer coefficient
n_1	Charge number
F	Faraday constant
E	Electric potential
R	Universal gas constant
T	Thermodynamic temperature
V_z	Normal flow velocity
c	Concentration
z	Distance from electrode surface
ω	Rotation rate (angular velocity)
γ	Dynamic viscosity
D	Diffusion coefficient
J	Diffusion rate
i	Current density

Anode limiting current was generated because at a certain critical current density, $CuCl^-_{ads}$ produced by reaction (A-1) could directly lose electrons in the absence of the action of Cl^- to generate $CuCl_{ads}$ (reaction B2-1). $CuCl_{ads}$ further formed $CuCl$ film, i.e. reaction (B2-2), while $CuCl$ film hindered the electrochemical reaction and mass transfer process. Dissolution process of $CuCl$ film under the complexation of Cl^- was precisely reaction (C-1). Initially, $CuCl$ production rate was greater than the rate of complexation by Cl^- , so that $CuCl$ could be effectively accumulated. With increasing amounts of $CuCl$ accumulation, $CuCl$ production rate slowed down to be consistent with the $CuCl$ complexation dissolution rate and the diffusion rate of resulting $CuCl_2^-$, so as to establish an equilibrium. Therefore, limiting current was controlled by $CuCl_2^-$ diffusion process, and the limiting current generating mechanism was essentially the diffusion-controlled film dissolution mechanism.

Symbols used in this section are shown in Table 1.

Based on reaction (C-1), CuCl_2^- production rate by film dissolution could be obtained. Since CuCl had already formed a layer of film, its concentration was 1:

$$r_{\text{CuCl}_2^-} = k_4[\text{Cl}^-] - k_{-4}[\text{CuCl}_2^-] \quad (1)$$

Diffusion process of CuCl_2^- conformed to the convection-diffusion equation:

$$V_z(z) \frac{dc}{dz} = D \frac{d^2c}{dz^2} \quad (2)$$

In this section, c represented the CuCl_2^- concentration, while D was the diffusion coefficient of CuCl_2^- . z was the vertical distance to the electrode surface; V_z was the velocity of water in the vertical direction on electrode surface; and $V_z(z)$ denoted that the flow velocity was a function of z [33]. ω was the rotation rate, whereas γ was the dynamic viscosity of solution.

$$V_z(z) \approx -0.51\omega^{3/2}\gamma^{-1/2}z^2 \quad [33] \quad (3)$$

Next, the convection-diffusion equation was solved. Let $\frac{dc}{dz} = m$, the following could be

obtained by integrating (2):

$$\ln \frac{m}{k} = \frac{1}{D} \int_0^z V_z(z) dz \quad (4)$$

Equation (4) could be rewritten as an exponential form:

$$m = \frac{dc}{dz} = k \exp \left[\frac{1}{D} \int_0^z V_z(z) dz \right] \quad (5)$$

When $z = 0$, we have:

$$k = \left(\frac{dc}{dz} \right)_{z=0} \quad (6)$$

By reintegrating equation (5), the following was obtained (for the distinction between the two integrations, z in the first integration was written as y):

$$c = k \int_0^z \exp \left[\frac{1}{D} \int_0^y V_y(y) dy \right] dz + B \quad (7)$$

B was a constant.

Boundary condition 1: When $z = \infty$, $c = 0$, then

$$B = -k \int_0^\infty \exp \left[\frac{1}{D} \int_0^y V_y(y) dy \right] dz \quad (8)$$

By substituting (8) into (7), complete expression for CuCl_2^- concentration was obtained:

$$c = k \int_0^z \exp \left[\frac{1}{D} \int_0^y V_y(y) dy \right] dz - k \int_0^\infty \exp \left[\frac{1}{D} \int_0^y V_y(y) dy \right] dz \quad (9)$$

On the electrode surface (i.e. at $z = 0$), CuCl_2^- concentration was:

$$c_{z=0} = -k \int_0^\infty \exp \left[\frac{1}{D} \int_0^y V_y(y) dy \right] dz \quad (10)$$

The above formula contained an integral form, namely

$$\int_0^\infty \exp\left[\frac{1}{D} \int_0^y V_y(y) dy\right] dz \quad (11)$$

Integral term in the exponential part of (15) was calculated first as follows

$$\int_0^y V_y(y) dy \quad (12)$$

By substituting (3) into (12), the following was obtained:

$$\int_0^y V_y(y) dy = -0.51\omega^{3/2}\gamma^{-1/2} \int_0^y y^2 dy = -\frac{0.51\omega^{3/2}\gamma^{-1/2}y^3}{3} \quad (13)$$

By substituting (13) into (11), the following was obtained:

$$\int_0^\infty e^{-bz^3} dz = \int_0^\infty e^{-(b^{1/3}z)^3} dz = \frac{1}{b^{1/3}} \int_0^\infty e^{-(b^{1/3}z)^3} d(b^{1/3}z) \quad (14)$$

Where $b = \frac{0.51\omega^{3/2}\gamma^{-1/2}}{3D}$. Assuming that $x = b^{1/3}z$, then equation (14) was written as

$$\frac{1}{b^{1/3}} \int_0^\infty e^{-x^3} dx = \frac{1}{3b^{1/3}} \int_0^\infty e^{-x^3} (x^3)^{-2/3} dx^3 \quad (15)$$

Given $t = x^3$, then (15) was written as

$$\frac{1}{3b^{1/3}} \int_0^\infty e^{-t} t^{-2/3} dt = \frac{1}{b^{1/3}} \Gamma\left(\frac{4}{3}\right) = 1.62D^{1/3}\omega^{-1/2}\gamma^{1/6} \quad (16)$$

Where $\Gamma(x)$ was the gamma function, $\Gamma(4/3) = 0.8934$. Expression of integral form (11) was precisely equation (16), thus

$$\int_0^\infty \exp\left[\frac{1}{D} \int_0^y V_y(y) dy\right] dz = 1.62D^{1/3}\omega^{-1/2}\gamma^{1/6} \quad (17)$$

By substituting (17) into (10), the following was obtained:

$$c_{z=0} = -1.62kD^{1/3}\omega^{-1/2}\gamma^{1/6} \quad (18)$$

Boundary condition 2: When $z = 0$, CuCl_2^- diffusion rate $J_{\text{CuCl}_2^-,z=0}$ could be described by Fick's first law because of the stiction effect. Moreover, electrode surface normal direction was opposite to the direction of CuCl_2^- concentration gradient, hence:

$$J_{\text{CuCl}_2^-,z=0} = D \left(\frac{dc}{dz} \right)_{z=0} = Dk \quad (19)$$

Regardless of whether the reaction was diffusion controlled or electrochemically controlled, in steady equilibrium state, CuCl_2^- production rate $r_{\text{CuCl}_2^-,z=0}$ was equal to the CuCl_2^- diffusion rate $J_{\text{CuCl}_2^-,z=0}$ at $z = 0$. Besides, the two were opposite in direction.

$$J_{\text{CuCl}_2^-,z=0} = Dk = -r_{\text{CuCl}_2^-,z=0} \quad (20)$$

By substituting (1) into (20), the following was obtained:

$$Dk = k_{-4} [\text{CuCl}_2^-]_{z=0} - k_4 [\text{Cl}^-] \quad (21)$$

By substituting (18) into (21), the following was obtained:

$$k = -\frac{k_4[\text{Cl}^-]}{D + 1.62k_{-4}D^{1/3}\omega^{-1/2}\gamma^{1/6}} \quad (22)$$

Current i could be represented by the diffusion rate $J_{\text{CuCl}_2, z=0}$ of CuCl_2^- at $z = 0$. Since the anode current direction was consistent with the diffusion direction of CuCl_2^- :

$$i = n_1 F J_{\text{CuCl}_2, z=0} = -FD \left(\frac{dc}{dz} \right)_{z=0} = -FDk = Fk_4[\text{Cl}^-] \frac{0.62D^{2/3}\omega^{1/2}\gamma^{-1/6}}{k_{-4} + 0.62D^{2/3}\omega^{1/2}\gamma^{-1/6}} \quad (23)$$

Where n_1 was the number of charges ($n_1 = -1$) carried by CuCl_2^- .

As can be seen from the above equation, current i was independent of potential E in the limiting current region, which was evident from various polarization curves. When temperature T rose, diffusion coefficient D and current i increased, which were consistent with the results in Figure 7. In addition, equations (24) and (25) derived from (23) coincided with the results in Figures 4 and 6, respectively.

$$\frac{d \log i}{d \log [\text{Cl}^-]} = 1 \quad (24)$$

$$\frac{d \log i}{d \log \omega} \leq 0.5 \quad (25)$$

Therefore, the mathematical model could effectively reflect the electrochemical behavior of coating in the anode limiting current region.

Many researches have been done to studied the electrochemical behavior of copper in NaCl solution, and three different reaction mechanisms and corresponding mathematical models of Tafel region were developed. There are many researches involved the limiting current, and a small number of them proposed the relevant polarization kinetic equations and mathematical models. For example, Moreau [25] and J. Wang [10] studied the electrochemical polarization behavior in limiting current region of copper in stationary seawater and the relevant polarization kinetic equation in stationary seawater environments was proposed:

$$i_L = Fk_4[\text{Cl}^-] \quad (26)$$

$$i_L = FD \frac{k_4}{D + k_{-4}\delta} [\text{Cl}^-] \quad (27)$$

Equation 27 is an approximation of equation 23 with the condition of ω tends to zero, and equation 26 is further approximations of equation 27 when the reaction C-1 is regarded as equilibrium. Therefore, the kinetic equation 23 of the rotating electrode can not only reflect the static solution environment, but also reflect the dynamic solution environment. It is more universal.

4. CONCLUSION

Under strong convection and high temperature conditions, cumulative effect of insoluble corrosion product CuCl weakened, corrosion current increased, and current peak disappeared gradually due to enhanced diffusion. Limiting current i_L and rotation rate ω were in a log-linear relationship. When the Cl^- concentration in the solution increased, large amounts of Cl^- were complexed with insoluble CuCl to generate soluble CuCl_2^- . Thus, limiting current increased, potential range of limiting current narrowed, and current peak disappeared gradually. Limiting current was also in a log-linear

relationship with the Cl^- concentration. As cathode, Cu_2O particles in the coating promoted the corrosion of copper and the release of dissolved copper, which improved the antifouling efficacy of the coating. Limiting current was controlled by diffusion process of CuCl_2^- , and the limiting current generating mechanism was essentially the diffusion-controlled film dissolution mechanism. The mathematical model for limiting current region 1 was built based on the reaction course proposed herein agreed well with the experimental results, which proved the correctness of the reaction course hypothesis and the mathematical model.

References

1. R. Ding, X. B. Li, J. Wang and L. K. Xu, *Paint Coat. Ind.*, 44 (2014) 5.
2. R. Ding, X. B. Li, J. Wang and L. K. Xu, *Mater. Rev.*, 26 (2012) 13.
3. R. A. Horne, *Syll. Epi. Barc.*, 577 (1952) 109.
4. S. N. Ma and Z. P. Zhang, *Chi. Surf. Eng.*, 22 (2009) 19.
5. A. P. Alkimov, V. F. Kosarev and A. N. Papyrin, *Dokl. Akad. Nauk.*, 315 (1990) 1062.
6. R. E. Blose and T. J. Roemer, *Proc. Int. Therm. Spr. Conf.*, 1 (2003) 103.
7. J. Karthikeyan and C. M. Kay, *Proc. Int. Therm. Spr. Conf.*, 1 (2003) 117.
8. T. Stoltenhoff, H. Kreye and H. J. Richter, *J. Therm. Spr. Tech.*, 11 (2002) 542.
9. R. Ding, X. B. Li, J. Wang and L. K. Xu, *Int. J. Electrochem. Sci.*, 8 (2013) 5902.
10. R. Ding, X. B. Li, J. Wang and L. K. Xu, *Chi. J. Mater. Res.*, 27 (2013) 212.
11. J. Chen, Z. Qin and D. W. Shoosmith, *Corr. Eng. Sci. Tech.*, 46 (2011) 138.
12. J. E. Lee, H. D. Lee and G. E. Kim, *Environ. Eng. Res.*, 17 (2012) 17.
13. M. M. Antonijevic and M. B. Petrovic, *Int. J. Electrochem. Sci.*, 3 (2008) 1.
14. M. Yeganeh and M. Saremi, *Micro. Nano. Lett.*, 6(2011) 26.
15. D. Digby, S. Sharifi and J. Linder, *Meet. Abstr.*, 2 (2011) 1748.
16. H. P. Lee and K. Nobe, *J. Electrochem. Soc.*, 133 (1986) 2035.
17. X. N. Liao, F. H. Cao, L. Y. Zheng and et al., *Corr. Sci.*, 53 (2011) 3289.
18. M. Braun and K. Nobe, *J. Electrochem. Soc.*, 126 (1979) 1666.
19. G. Bianchi, G. Fiori, P. Longhi and F. Mazza, *Corr.*, 34 (1978) 396.
20. G. Faita, G. Fiori and D. Salvatore, *Corr. Sci.*, 15 (1975) 383.
21. A. L. Bacarella and J. C. Griess, *J. Electrochem. Soc.*, 120 (1973) 459.
22. S. R. de Sanchez and D. J. Schiffrin, *Corr. Sci.*, 22 (1982) 585.
23. W. H. Smyrl, *J. Electrochem. Soc.*, 132 (1985) 1556.
24. C. Deslouis, B. Tribollet, G. Mengoli and M. Musiani, *J. App. Electrochem.*, 18 (1988) 374.
25. A. Moreau, *Electrochimica Acta*, 26 (1981) 497.
26. B. Tribollet and J. Newman, *J. Electrochem. Soc.*, 131 (1984) 2780.
27. G. Kear, F. C. Walsh, D. B. Barker, K. S. Stokes, *Leighton Buzzard*, UK (2000).
28. M. E. Walton and P. A. Brook, *Corr. Sci.*, 17 (1977) 317.
29. M. Georgiadou and R. Alkire, *J. App. Electrochem.*, 28 (1998) 127.
30. F. King, M. J. Quin and C. D. Litke, *J. Electroanal. Chem.*, 385 (1995) 45.
31. R.K. Flatt and P.A. Brook, *Corr. Sci.*, 11 (1971) 185.
32. Schmidt T, Gartner F and Assadi H, *Acta. Mater.*, 54 (2005) 729.
33. V. G. Levich and C. W. Tobias, *J. Electrochem. Soc.*, 110 (1963) 251.